

1 **Supplementary Information:**

2 **Large tunability in the mechanical and thermal properties of carbon**
3 **nanotube-fullerene hierarchical monoliths**

4 Ashutosh Giri,^{1,*} John Tomko,² John T. Gaskins,¹ and Patrick E. Hopkins^{1,2,3,†}

5 ¹*Department of Mechanical and Aerospace Engineering,*
6 *University of Virginia, Charlottesville, Virginia 22904, USA*

7 ²*Department of Materials Science and Engineering,*
8 *University of Virginia, Charlottesville, Virginia 22904, USA*

9 ³*Department of Physics, University of Virginia, Charlottesville, Virginia 22904, USA*

10 To assess the thermodynamic structural stability for our fullerene-nanotube nanotruss sys-
11 tems, we perform density functional theory calculations using the quantum espresso package.¹
12 The Perdew-Zunger exchange correlation functional is used to calculate the total binding energies
13 of our systems. The structures are optimized according to the ionic relaxation calculation with
14 an energy convergence threshold of 0.0001 Ryd and a convergence threshold for forces of 0.001
15 Ryd/Bohr. The cohesive energies are determined by calculating the difference between the ener-
16 gies of structures compared to the energy of a single carbon atom using the same pseudo potential
17 and calculation parameters with $6 \times 6 \times 6$ Monkhorst-Pack k-point set. The calculated cohesive
18 energy for our (6,0) CNT is 8.45 eV/atom and the cohesive energies for our nanotruss structures
19 range from 8.20 to 8.27 eV/atom, which indicates that our structures are thermodynamically stable.
20 We note that similar first principles calculations have shown that fullerene-nanotube structures can
21 be designed by connecting icosahedral symmetry fullerenes (C_{240} , C_{320} and C_{500}) and (6,6) nan-
22 otube, which can form thermodynamically stable 3D structures.² However, in this work, we only
23 consider structures that can be designed via the [6+6] cycloaddition since such additions have been
24 studied in detail both theoretically and experimentally.^{3,4} As such, the C_{80} and (6,0) CNT provides
25 a unique combination to design these 3D hierarchical monoliths due to symmetry considerations.

26 All structures are equilibrated under isothermal-isobaric ensemble (NPT integration) with the
27 number of particles, pressure and temperature of the system held constant for a total of 2 ns at 0
28 bar pressure. This allows the stress in the structure to relax. Following NPT integration, an NVT
29 integration at the prescribed temperature, which is the Nose-Hoover thermostat⁵ with the number
30 of atoms, volume and temperature of the simulation held constant is enforced to fully equilibrate
31 the structures at that temperature for another 1 ns. After equilibration, we apply a uniaxial strain to
32 calculate the stress-strain relation or we apply the Green-Kubo approach to calculate the thermal
33 conductivity for the structure. For all simulations, we use the AIREBO potential with a cutoff
34 of 2 Å since it has been shown that a lower cutoff distance of 1.7 Å can result in significantly
35 overestimated mechanical properties in graphene.⁶

36 To calculate the stress-strain relationship, the simulation cell is deformed in the x -direction
37 at a strain rate of 10^8 s^{-1} . In the y - and z -directions, we impose zero pressure at these lateral
38 boundaries under the NPT integration. The strain is calculated every 0.1 ps as, $L_x - L/L$, where
39 L_x is the current length in direction of the applied strain and L is the initial length of in the same
40 direction. The stress of the entire structure is also outputted every 0.1 ps to generate a stress-
41 strain relationship for the structures. We have also performed additional tensile simulations with

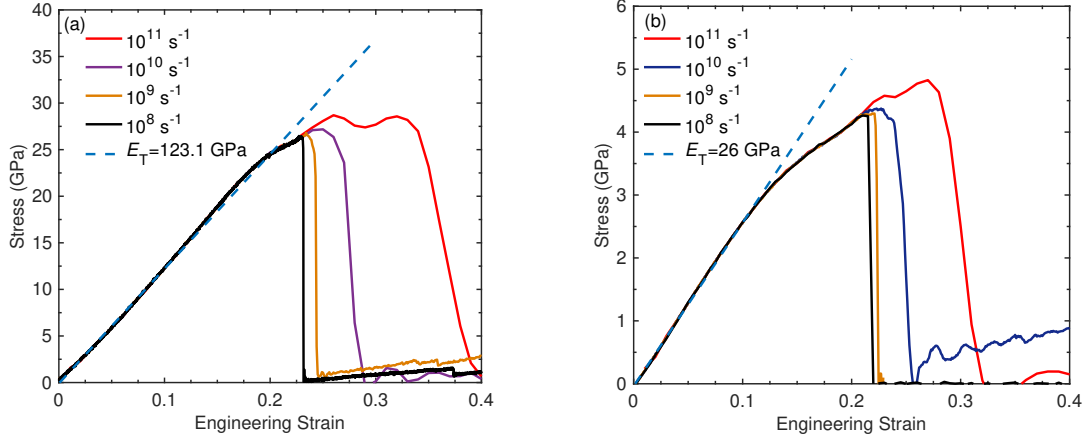


Figure S1. (a) Stress-strain curves at varying strain rates for CNT-fullerene nanotruss structures with (a) $d=7.0 \text{ \AA}$ and (b) $d=28.0 \text{ \AA}$.

42 varying strain rates as shown in Fig. S1. Increasing the strain rate from 10^8 s^{-1} to 10^{11} s^{-1} has
 43 negligible influence on the Young's modulus, whereas, the fracture strain and fracture strength
 44 are increased due to higher strain rates. This is in line with previous simulations of tensile strain
 45 rate dependence for graphene and graphyne as shown in Ref. 6. The increased ductility at higher
 46 strain rates has been attributed to localization of buckling and significantly reduced recoverability
 47 in CNT bundles.⁷

48 We calculate the bond lengths for our structure with $d=17.5 \text{ \AA}$ at different strain levels to elu-
 49 cidate the effect of sp^3 -like C–C bonds on the mechanical response of the structures to uniaxial
 50 loading. For the unstrained case as shown in Fig. S2a, we calculate an average bond length of
 51 $\sim 1.55 \text{ \AA}$, whereas the average bond length for the sp^2 -like C–C bonds is 1.43 \AA . During uniax-
 52 ial tensile loading, the sp^3 bonds that are formed at the connection between the fullerene and the
 53 CNT show drastic increase in bond lengths as shown in Fig. S2b for $\varepsilon=0.1$. The increased sp^3 -
 54 like bond lengths indicate that stress concentration occurs around the bonds formed between the
 55 fullerene and the CNT. However, for $\varepsilon=0.2$ where ductile deformation initiates, the bond lengths
 56 in the entire CNT along the tensile loading direction increase considerably suggesting that stress
 57 propagates along the nanotube in the direction of the applied strain and ultimately leads to frac-
 58 ture. Similarly, for the case of uniaxial compressive loading, the sp^3 C–C bonds are the ones that
 59 are elongated the most as shown in Fig. S2d and Fig. S2e. In contrast to tensile loading, the sp^3
 60 C–C bonds bend due to compressive loading, which leads to the eventual collapse of the cells and

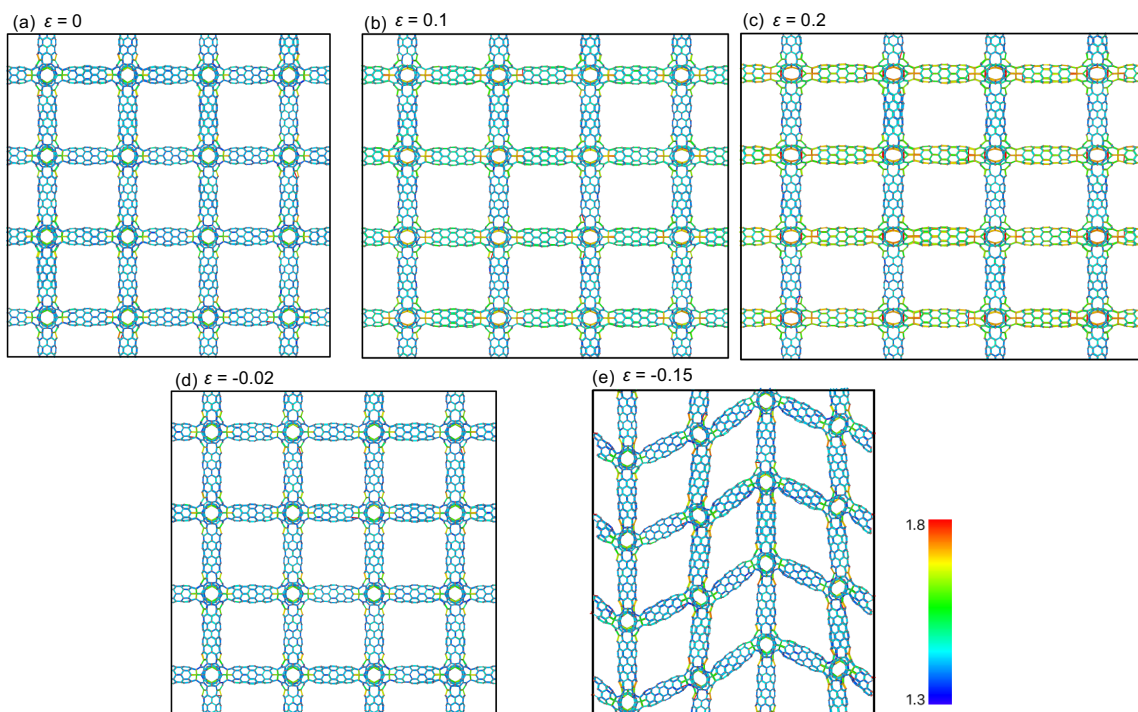


Figure S2. (a) Snapshots of cross sections showing calculations of bond lengths at varying strain rates for CNT-fullerene nanotruss structures with $d=17.5 \text{ \AA}$ under uniaxial tensile loading at (a) $\epsilon=0$, (b) $\epsilon=0.1$ and (c) $\epsilon=0.2$. Similarly, snapshots at (d) $\epsilon=0.02$ and (e) $\epsilon=0.15$ under uniaxial compression. The color bar represents bond lengths from 1.3 to 1.8 \AA .

61 densification of the structures.

62 Figure S3 shows the bond length calculations for the C_{80} molecules in the above mentioned
 63 structure. We note that, 45 % of the carbon atoms in the fullerene are involved with sp^3 -like C–C
 64 bonds with an average bond length of 1.55 \AA as shown in Fig. S3a for an unstrained fullerene
 65 molecule in a CNT-fullerene structure with $d=17.5 \text{ \AA}$. For the uniaxial tensile loading case, only
 66 the sp^3 -like bonds in the fullerenes show increased bond lengths as shown in Fig. S3b for $\epsilon=0.1$.
 67 As the tensile strain is increased further, the fullerene molecules in the structures elongate in the
 68 direction of the applied strain. However, for the compressive loading case, the fullerene molecules
 69 do not show deformation until the CNTs start to bend, which deforms the C_{80} molecules as shown
 70 in Figs. S3e and S3f. These comparisons between the tensile and compressive loading cases
 71 (along with the bond length comparisons for the whole CNT-fullerene nanotruss structures) help
 72 explain the different stress-strain behaviors for the two loading cases.

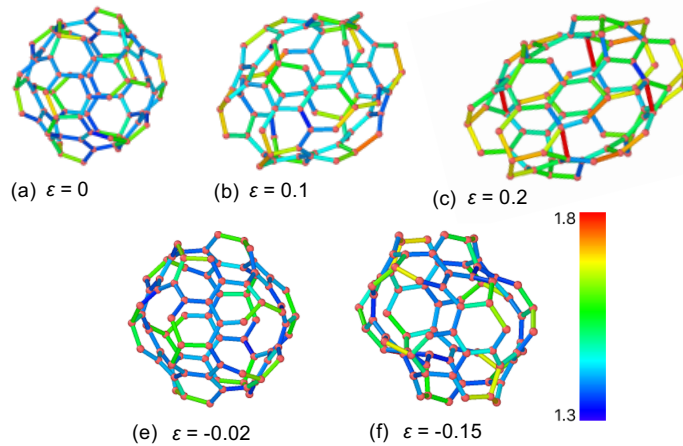


Figure S3. (a) Snapshots of C₈₀ molecules showing calculations of bond lengths at varying strain rates for CNT-fullerene nanotruss structures with $d=17.5 \text{ \AA}$ under uniaxial tensile loading at (a) $\epsilon=0$, (b) $\epsilon=0.1$ and (c) $\epsilon=0.2$. Similarly, snapshots of bond lengths for only the fullerene molecules at (d) $\epsilon=0.02$ and (e) $\epsilon=0.15$ under uniaxial compression. The color bar represents bond lengths from 1.3 to 1.8 \AA .

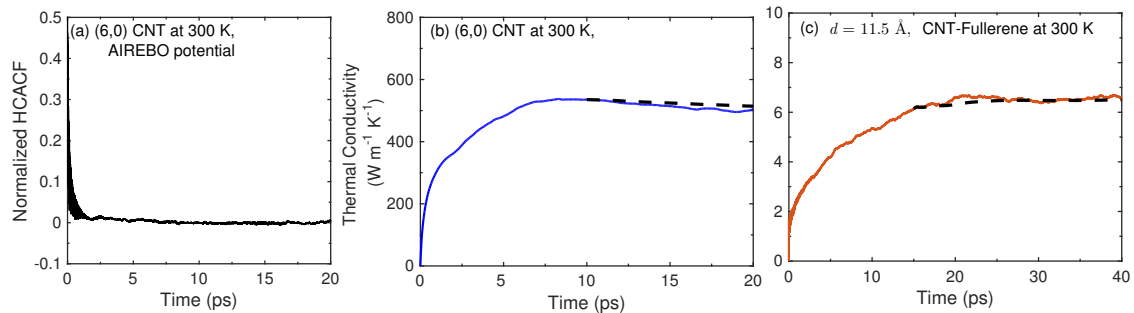


Figure S4. (a) The calculated HCACF as a function of time for a (6,0) CNT at room temperature. Converged value of thermal conductivity for a (b) (6,0) CNT, and for a (c) CNT-fullerene nanotruss with $d=11.5 \text{ \AA}$ calculated from the integral of the heat current autocorrelation function for a total of 20 ps and 40 ps, respectively at room temperature.

73 For the Green-Kubo (GK) method under the equilibrium molecular dynamics simulation frame-
 74 work, the thermal conductivity of our CNT-fullerene structures in the α th direction (which we
 75 calculate for the x -, y -, and z -directions, see Fig. 1) is given by,

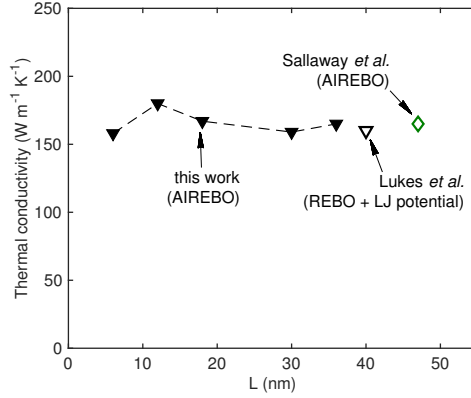


Figure S5. Thermal conductivity of (9,9) single-walled CNT as a function of length, L , predicted via the Green-Kubo approach (solid symbols) with the AIREBO potential. The thermal conductivity of single-walled CNT predicted via MD taken from Lukes *et al.*⁸ and Salaway *et al.*⁹ along with their respective potentials used are also shown for comparison.

$$\kappa_{\alpha} = \frac{1}{k_{\text{B}}VT^2} \int_0^{\infty} \langle S_{\alpha}(t)S_{\alpha}(0) \rangle dt, \quad (1)$$

76 where t is the time, T and V are the temperature and volume of the system under consideration,
77 respectively, and $\langle S_{\alpha}(t)S_{\alpha}(0) \rangle$ is the α th component of the heat current autocorrelation function
78 (HCACF).^{10–13} The heat current is calculated every 10 time steps during the data collection period
79 and the integration of the HCACF is carried out till the HCACF completely decays to zero, which
80 depends on the simulation domain. An example of the calculated HCACF as a function of time
81 for a (6,0) SWCNT is shown in Fig. S4a where the HCACF decays to zero by 5 picosecond but
82 the thermal conductivity is calculated from the average of integral of the HCACF from 10 ps to 20
83 ps to get a converged value as shown in Fig. S4b. The equilibrium MD simulations can result in
84 size effects affecting the thermal conductivities if all available vibrational modes are not accounted
85 for in the simulation domain.¹⁴ Therefore, we conduct GK simulations on different domains sizes,
86 $L \times L \times L$, to check for finite size effects in our simulations.

87 To gain more confidence in our thermal conductivity predictions, we compare the results for
88 single-walled CNTs of various lengths with those that are reported in literature, which have im-
89 plemented similar interatomic potentials. Figure. S5 shows that our thermal conductivities for
90 different domain lengths of (9,9) CNT predicted from the GK method match very well with prior

91 results for single-walled CNT with similar chirality, length and interatomic potentials.

92 * ag4ar@virginia.edu

93 † phopkins@virginia.edu

94 ¹ P. Giannozzi, S. Baroni, N. Bonini, M. Calandra, R. Car, C. Cavazzoni, D. Ceresoli, G. L. Chiarotti,
95 M. Cococcioni, I. Dabo, A. D. Corso, S. de Gironcoli, S. Fabris, G. Fratesi, R. Gebauer, U. Gerstmann,
96 C. Gougoussis, A. Kokalj, M. Lazzeri, L. Martin-Samos, N. Marzari, F. Mauri, R. Mazzarello, S. Paolini,
97 A. Pasquarello, L. Paulatto, C. Sbraccia, S. Scandolo, G. Sclauzero, A. P. Seitsonen, A. Smogunov,
98 P. Umari, and R. M. Wentzcovitch, *Journal of Physics: Condensed Matter* **21**, 395502 (2009).

99 ² W. M. Ji, L. W. Zhang, and K. M. Liew, *EPL (Europhysics Letters)* **121**, 56001 (2018).

100 ³ X. Wu and X. C. Zeng, *ACS Nano* **2**, 1459 (2008).

101 ⁴ A. G. Nasibulin, P. V. Pikhitsa, H. Jiang, D. P. Brown, A. V. Krasheninnikov, A. S. Anisimov, P. Queipo,
102 A. Moisala, D. Gonzalez, G. Lientschnig, A. Hassanien, S. D. Shandakov, G. Lolli, D. E. Resasco,
103 M. Choi, D. Tománek, and E. I. Kauppinen, *Nature Nanotechnology* **2**, 156 (2007).

104 ⁵ W. G. Hoover, *Phys. Rev. A* **31**, 1695 (1985).

105 ⁶ Y.-Y. Zhang, Q.-X. Pei, Y.-W. Mai, and Y.-T. Gu, *Journal of Physics D: Applied Physics* **47**, 425301
106 (2014).

107 ⁷ S. Pathak, E. J. Lim, P. Pour Shahid Saeed Abadi, S. Graham, B. A. Cola, and J. R. Greer, *ACS Nano*
108 **6**, 2189 (2012), PMID: 22332591, <https://doi.org/10.1021/nn300376j>.

109 ⁸ J. R. Lukes and H. Zhong, *Journal of Heat Transfer* **129**, 705 (2006).

110 ⁹ R. N. Salaway and L. V. Zhigilei, *International Journal of Heat and Mass Transfer* **70**, 954 (2014).

111 ¹⁰ M. P. Allen and D. J. Tildesley, *Computer simulation of liquids (Oxford Science Publications)*, reprint
112 ed., Oxford science publications (Oxford University Press, 1989).

113 ¹¹ A. McGaughey and M. Kaviani, *International Journal of Heat and Mass Transfer* **47**, 1783 (2004).

114 ¹² A. McGaughey and M. Kaviani, *International Journal of Heat and Mass Transfer* **47**, 1799 (2004).

115 ¹³ A. J. H. McGaughey, *Phonon Transport in Molecular Dynamics Simulations: Formulation and Thermal*
116 *Conductivity Prediction*, Ph.D. thesis, University of Michigan (2004).

117 ¹⁴ J. M. Larkin and A. J. H. McGaughey, *Phys. Rev. B* **89**, 144303 (2014).